# High-frequency gravitational waves detection with the BabyIAXO haloscopes

José Reina-Valero,[1,*] Jose R. Navarro-Madrid,[2] Diego Blas,[3,4] Alejandro Díaz-Morcillo,[2] Igor García Irastorza,[5] Benito Gimeno,[1] and Juan Monzó-Cabrera[2]

[1]*Instituto de Física Corpuscular (IFIC), CSIC-University of Valencia, Calle Catedrático José Beltrán Martínez, 2, 46980 Paterna (Valencia), Spain*
[2]*Departamento de Tecnologías de la Información y las Comunicaciones, Universidad Politécnica de Cartagena, Plaza del Hospital 1, 30302 Cartagena, Spain*
[3]*Institut de Física d'Altes Energies (IFAE), The Barcelona Institute of Science and Technology, Campus UAB, 08193 Bellaterra (Barcelona), Spain*
[4]*Institució Catalana de Recerca i Estudis Avançats (ICREA), Passeig Lluís Companys 23, 08010 Barcelona, Spain*
[5]*Center for Astroparticles and High Energy Physics (CAPA), Universidad de Zaragoza, Zaragoza 50009, Spain*

(Received 10 August 2024; accepted 24 December 2024; published 13 February 2025)

We present the first analysis using RADES-BabyIAXO cavities as detectors of high-frequency gravitational waves (HFGWs). In particular, we discuss two configurations for distinct frequency ranges of HFGWs: cavity 1, mostly sensitive at a frequency range of 252.8–333.2 MHz, and cavity 2, at 2.504–3.402 GHz, which is a scaled down version of cavity 1. We find that cavity 1 will reach sensitivity to strains of the HFGWs of order $h_1 \sim 10^{-21}$, while cavity 2 will reach $h_2 \sim 10^{-20}$. These represent the best estimations of the RADES-BabyIAXO cavities as HFGW detectors, showing how this setup can produce groundbreaking results in axion physics and HFGWs simultaneously.

DOI: 10.1103/PhysRevD.111.043024

## I. INTRODUCTION

After their first direct discovery in 2015 by the LIGO collaboration [1] in the 100 Hz band, gravitational waves (GWs) are reshaping our understanding of the cosmos. More concretely, these messengers bring new information from previously undetectable events, and may be the key to access the most primordial instances of the Universe. When one considers the extraordinary progress in cosmology and astrophysics when the whole spectrum of electromagnetic (EM) radiation was used to explore the Universe, it is hard to think what may happen when GWs in a broad spectrum of frequencies will be discovered.

Out of the different possibilities, the "high frequency" band of GWs has recently received increasing attention [2]. Different reasons explain the current interest: first, the signals above the band of groundbase detectors (few kHz) are not highly populated by known astrophysical events, leaving a rich landscape of possible signals beyond the standard model to search for without foregrounds; second, higher frequency means smaller and faster devices, more compatible with laboratory scales, where one can leverage the revolution in sensing to look for these feeble signals.

From the universal coupling of gravitation, the possibilities to search for HFGWs in the sensing frontier are multifold. In this work, we will focus on one of the most promising ones: their impact on microwave electromagnetic cavities immersed in an intense magnetostatic field. A GW propagating along an intense static magnetic field can convert into an electromagnetic wave of the same frequency [3,4]. If this happens inside a cavity of the right size, this signal will accumulate, allowing the eventual detection of the primordial signal. This simple idea has been recently discussed in detail in [5–7]. The final sensitivity depends not only on the ability to detect tiny EM fields, but also on properties of the cavity, such as its volume or quality factor. In this way, dark matter axion detection experiments that make use of microwave resonant cavities would constitute an ideal environment to probe for HFGWs simultaneously. The axion is the most elegant solution to the well-known strong *CP* (charge-parity) problem in the framework of QCD, being a pseudoscalar, spin zero particle which arises when broking the additional U(1) symmetry proposed by Peccei-Quinn [8,9] in order to

*Contact author: jose.reina@uv.es

solve this issue. The axion has a coupling to photons, implying that via the inverse Primakoff effect [10,11] they can decay to photons when applying a strong external magnetic field. If the generated photon is inside a cavity, it can be eventually detected as a rf (radio-frequency) signal. Several experiments have been proposed and developed during the past 30 years [12–18], and along this work we will focus on the BabyIAXO (preliminary stage of IAXO) magnet, deriving results for GWs of frequencies between 252.8 to 333.2 MHz and 2.504 to 3.402 GHz.

A novel approach to the problem will be performed since no system with tuning capability and ports for both axions and GWs has been studied yet. We shall discuss how to adapt the experimental setup to detect HFGWs, and perform a quantitative study on how well the available system couples to an incident HFGW. This study, involving a tuning system, is especially relevant for the detection of stationary sources, following the same philosophy as in the axion case. Hence, superradiant black holes and GW backgrounds are of special interest for this kind of setup [5].

This paper is organized as follows: first, a brief commentary about the BabyIAXO experiment is performed, explaining its setup and capabilities; second, the electromagnetic design of the cavity for the RADES-BabyIAXO haloscope as well as tuning system and ports is shown, discussing its geometry and advantages, and how to adapt the setup for the simultaneous detection of both dark matter axions and HFGWs. After this, a numerical calculation of the form factor between the HFGW and RADES-BabyIAXO cavities is made paying special attention to the several values that experimental parameters can adopt. In addition, a calculation of the sensitivity estimation is performed, and the expression for the scanning rate is obtained with a formulation similar to the dark matter axion case.

## II. THE BABYIAXO EXPERIMENT

The IAXO (International Axion Observatory) experiment is one of the most ambitious projects in axion searches, whose aim is to detect solar axions [19,20]. The intermediate stage, the BabyIAXO helioscope, will be built as a stepping stone for the experiment, and it will be composed of a cryostat and a dipole magnet with two bores of 0.7 meters in diameter and 10 meters in length, providing a transversal magnetostatic field of 2 T [21]. This magnet gives the opportunity, in addition to operating as a helioscope, to search for dark matter axions with haloscopes, and the RADES collaboration made a proposal to use resonant cavities at low frequencies to search for dark matter axions in the mass range of 1-2 μeV, expecting competitive values in terms of axion sensitivity [22]. To cover this mass range, four cavities were designed with a frequency tuning system that allows to shift the operational frequency during the data taking campaigns. Although these four cavities share the same shape, the main difference lies in the diameter, which is larger for the cavity operating at lower frequencies and smaller for the cavity operating at higher frequencies, all maintaining the same length of 5 meters. Therefore, two cavities can be placed in each bore during the measurement operation, giving the chance to search in parallel at different masses (using four different cavities), or enhance the sensitivity by summing coherently the signals (using four cavities with the same dimensions). These cavities will be set in a cryostat system based on cooling via cryocoolers and a closed helium circulation loop [23], in order to cool them down to 4.6 K. Plans to push this temperature down to tens of mK are set as part of the recently granted ERC-SyG *DarkQuantum* with dilution refrigerator (DL) technology. This will allow to effectively get noise figures close to the standard quantum limit with superconducting quantum interference devices (SQUIDs).

As mentioned above, the properties of the RADES-BabyIAXO haloscope allow for the search of HFGWs, which can be done during the axion measurement time by making small changes in the cavities designed for dark matter search. A novelty of RADES-BabyIAXO is its kind of tuning mechanism, which comes with its own challenges. Indeed, the introduction of this mechanism perturbs considerably the electromagnetic modal field structure inside the cavity and the coupling between the HFGW and the resonant system is strongly modified. As a result, the tuning system originally employed for scanning over a mass range of axions can be useful for a frequency sweep to detect HFGWs with different frequencies.

## III. ELECTROMAGNETIC DESIGN

The electromagnetic study of the RADES-BabyIAXO cavities was performed in [22], where a quasicylindrical shape was adopted in order to avoid the degeneration of the modes $TE_{111}$ and maximize the volume, but not to fill completely the bore in order to leave some space for cables and instrumentation at both sides. Two cavities are analyzed in this article: the first one is the lower-frequency cavity that has been designed to operate in the MHz range (vhf and uhf bands), called cavity 1, and the second one is a 10 times scaled-down version of the first cavity working at the GHz range (S-band), called cavity 2. This second cavity would not be used in RADES-BabyIAXO, but has been designed and manufactured as a test model of cavity 1 for the GHz range. The tuning system incorporated in both cavities consist of two metallic thin rectangular plates along the longitudinal axis that turn simultaneously, shifting the frequency of the operational EM mode. A schematic of the cavity geometry is shown in Fig. 1, while Table I contains the dimensions of the two designs.

It is well known that in dark matter axion experiments using a cylindrical cavity immersed within a dipole magnet, the resonant mode that provides the maximum coupling between the radio-frequency (rf) electric field and the external static magnetic field is the $TE_{111}$ mode, which

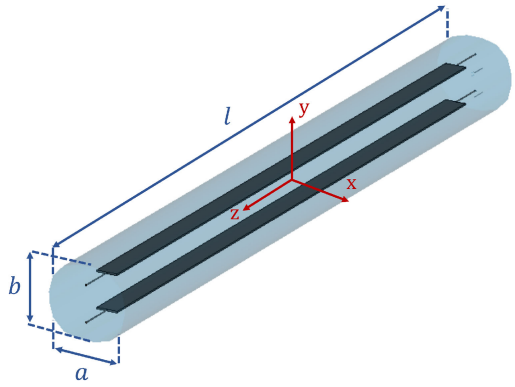


FIG. 1. Schematic of the RADES-BabyIAXO cavities geometry. The cavity (in blue color) has a quasicylindrical shape, with dimensions $a$ (width), $b$ (height), and $l$ (length), where the relation $b = 0.9a$ is fulfilled. The metallic rectangular plates for the frequency tuning are shown in dark gray color. The chosen reference frame in the center of the cavity is shown in red.

is a degenerate mode that, at the same resonant frequency, has two polarizations orthogonal to each other [24]. In the case of the RADES-BabyIAXO cavities, due to the presence of the plates and with the condition $a \neq b$, such degeneracy disappears and both modes, quasi-$TE_{111}$ with vertical and horizontal polarization, adopt two distinct frequencies.

In HFGW detection, the use of a second mode is of special interest, as the gravitational wave can couple not only to both modes [5,25], but it can excite them at the same time if the bandwidth of the HFGW is higher than the frequency gap between both modes. Thus, the modes analyzed in this article are the quasi-$TE_{111}$ with an initial vertical polarization (oriented to the $y$ axis in Fig. 1) and the quasi-$TE_{111}$ with an initial horizontal polarization (oriented in the $x$ axis), which we call mode 1 and mode 2, respectively; the rf electric field pattern in the cavity central plane $z = 0$ is plotted in Fig. 2 for both modes. These modes are affected differently by the tuning system, as it is shown in Fig. 3. Mode 1 decreases its resonant frequency when the plates are rotated, while mode 2 increases its resonant frequency. Note that the tuning range is smaller for mode 2 than for mode 1, being this range for mode 1, 43.33 and 523.5 MHz for cavities 1 and 2, respectively, compared to the range of mode 2, 29.74 and 327.5 MHz for cavities 1 and 2, respectively.

The possibility to change the resonant frequency of both modes gives the opportunity to search for HFGWs in a total

TABLE I. Dimensions and operational frequency range of the studied cavities. The thickness of both metallic plates is 1 cm.

| Cavity model | a (cm) | b (cm) | l (cm) | Frequency range |
|---|---|---|---|---|
| Cavity 1 | 56 | 50.4 | 500 | 252.8–333.2 MHz |
| Cavity 2 | 5.5 | 4.9 | 50 | 2.504–3.402 GHz |

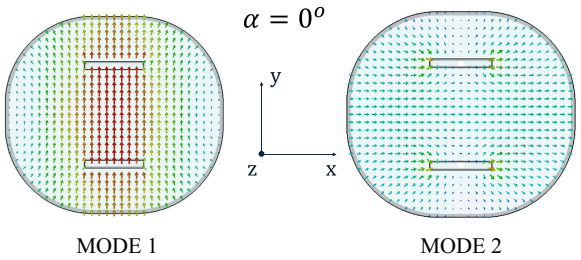


FIG. 2. Electric field profiles of mode 1 and mode 2 in a transversal cut of cavity 2 (also applicable to cavity 1) for plates angle $\alpha = 0°$. Size and color of the arrows indicate the magnitude of the electric field in linear (from more intense in red to weaker in blue).

range of 73.1 and 850.9 MHz for cavities 1 and 2, respectively. However, there is a frequency range where it is not possible to scan, and it corresponds to the frequency separation of both modes at the starting point, i.e., when the angle of the plates is 0°. To avoid this frequency gap, the cavity section should have a $b/a$ ratio around $b/a \approx 1$.

### A. Coupling ports

An important aspect of this experiment is how to couple the EM signals generated by the HFGW, as the position and type of port will determine which modes can be detected. The port, proposed in [22], is a coaxial loop located at one of the cavity ends that couples the magnetic field of mode 1. In order to couple mode 2, the same concept can be used although in this case the second coaxial loop is placed at the other end of the cavity and must be rotated 90° with respect to that of port 1 in order to couple to the mode 2 rf magnetic field. Figure 4 shows a schematic view of the location of the two ports in the haloscope, where port 1 is a coaxial loop oriented $\phi_1 = 90°$ with respect to the $XZ$ plane that couples mode 1. Port 2 is another coaxial loop oriented $\phi_2 = 0°$

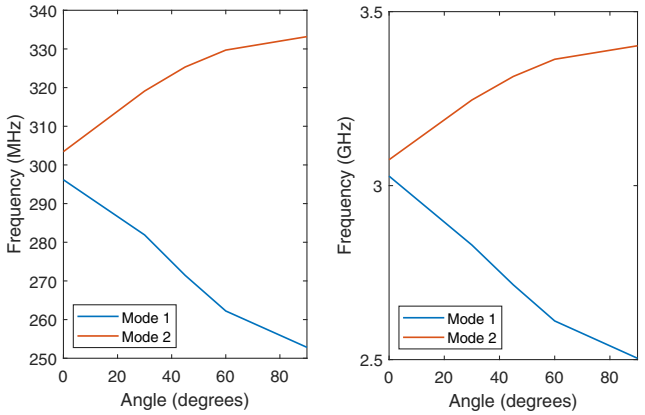


(a) (b)

FIG. 3. Resonant frequency variation during tuning versus plates angles for (a) cavity 1 and (b) cavity 2.

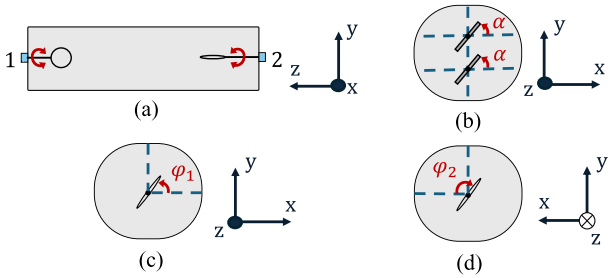


FIG. 4. Geometry of ports and plates inside the cavity. (a) Motion representation of the loops for rf magnetic field detection. (b) Definition of angle $\alpha$ of the plates with respect to the $x$ axis. (c),(d) Definition of angles $\varphi_1$ and $\varphi_2$ with respect to the $x$ axis.

with respect to the $XZ$ plane that couples mode 2. Rotation angles are denoted as $\varphi_1$ and $\varphi_2$ for ports 1 and 2, respectively. Both loops can be rotated in order to recouple during the frequency tuning process, that is, the coupling coefficient $\beta$ [24] can be varied by rotating the loops.

### B. Electromagnetic field change due to frequency tuning mechanism

To illustrate the structure of the electromagnetic field inside the cavities when the tuning plates and coaxial loops are rotated, Fig. 5 shows both the electric field profile in a cross section at the origin of the reference frame and the magnetic field around one of the coaxial loops. As can be observed in the $\vec{E}$ field row, the boundary conditions are fulfilled as should be expected, as well as in the case of the $\vec{H}$ row, where the coaxial loop must be rotated depending on the structure of the mode magnetic field (i.e., depending on the plates angle $\alpha$).

## IV. FORM FACTOR

This work is focused on the HFGW coupling to the cavity related to the Gertsenshtein effect [3,4]: GWs will convert into EM waves of the same frequency in the presence of a background very intense magnetostatic field. This coupling can be quantified by the following coupling factor given by [5]

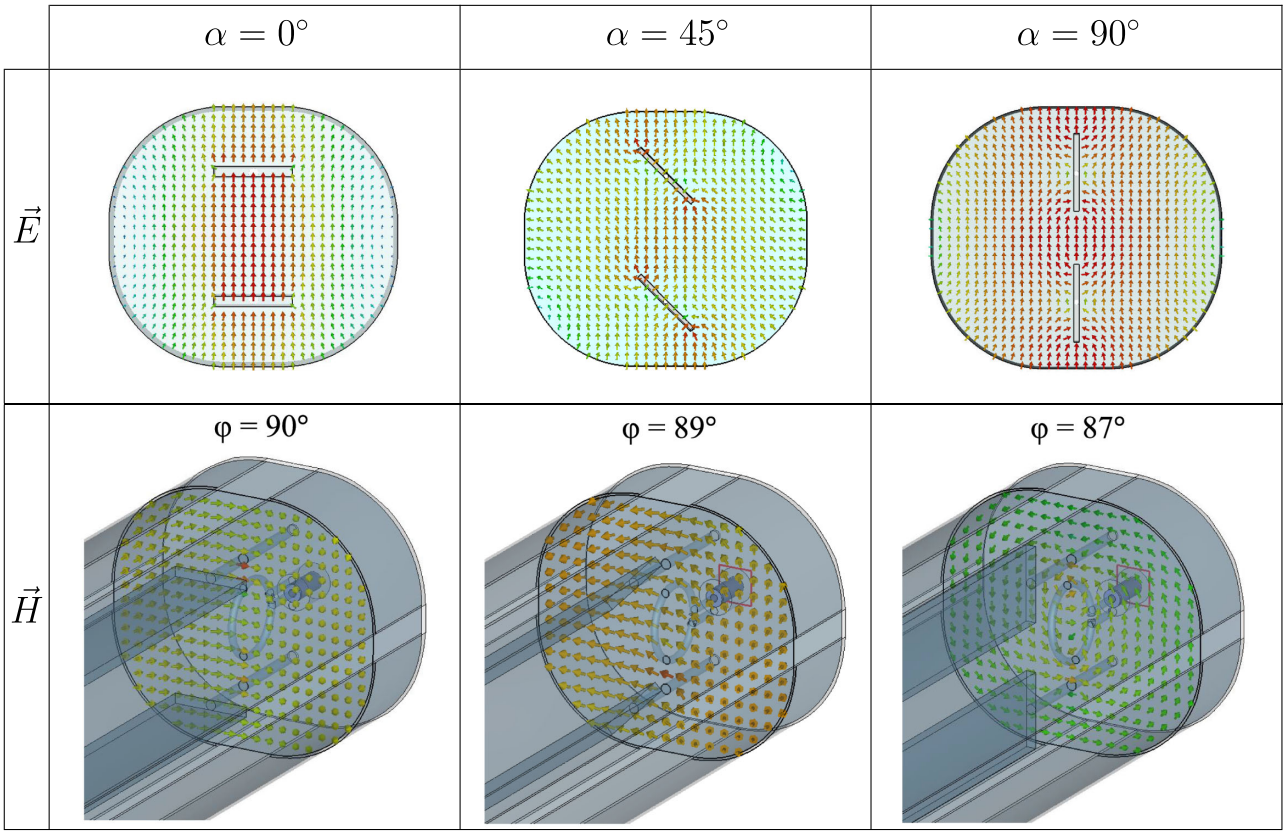


FIG. 5. Electromagnetic field structure inside cavity 1 for mode 1. Size and color of the arrows indicate the magnitude of the corresponding field in linear (from more intense in red to weaker in blue). A cross section of the electric field $\vec{E}$ is shown for different plates angles $\alpha$. In the same way, the magnetic field $\vec{H}$ is represented along port 2, where angle $\varphi$ of the loop is fixed in each case to obtain the required coupling.

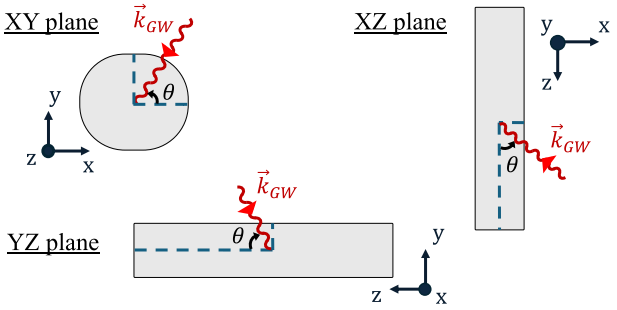


FIG. 6. Scheme of HFGWs incidence in each plane.

$$\tilde{\eta}_{m_{+,\times}} = \frac{|\int_V \vec{E}_m(\vec{r}) \cdot \vec{J}_{+,\times}(\vec{r}) \mathrm{d}V|}{V^{1/2} |\int_V \vec{E}_m(\vec{r}) \cdot \vec{E}_m(\vec{r}) \mathrm{d}V|^{1/2}}, \tag{1}$$

where $\vec{E}_m$ is the rf electric field of the $m$th resonant mode inside the cavity, $\vec{J}_{+,\times}$ the electric density current arisen by a monochromatic HFGW for plus and cross polarizations (see [5]), and $V$ the volume of the cavity.

From this expression, when both the electric field and density current are perfectly aligned, the form factor will have maximum magnitude. However, the expression of $\vec{J}$ is relatively complex, making it nontrivial to analyze its effect [26]. In particular, even though the static magnetic field is oriented along the $y$ axis, the HFGW can couple to any cavity mode with different magnitudes of the coupling factor. Therefore, it is of interest to perform a numerical calculation of $\tilde{\eta}_{m_{+,\times}}$ making a sweep in the angle of incidence of the HFGW (see Fig. 6), $\theta$, and fixing the remaining parameters to a given value. For this purpose, a simulation of the rf electromagnetic fields inside the cavity has been performed with the eigenmode solver of CST Studio Suite software [27].

The study is divided in the following cases: first, a given polarization of the HFGW (+ or ×) is selected; then, we study a given plane of incidence in order to define $\theta$ (defined with respect to the $z$ axis in the $XZ$, $YZ$ incidence planes and to the $x$ axis in the $XY$ incidence plane); finally, the tuning plates angle ($\alpha$) is fixed to a given value, defined with respect to the $x$ axis. Results for the mode 1 of cavity 1 are shown in Fig. 7. Different values of $\alpha$ (0°, 30°, 45°, 60°, and 90°) have been chosen in order to sweep the main region of interest in which the structure of the electric field is modified considerably. Any result of $\tilde{\eta}_{m_{+,\times}}$ associated to

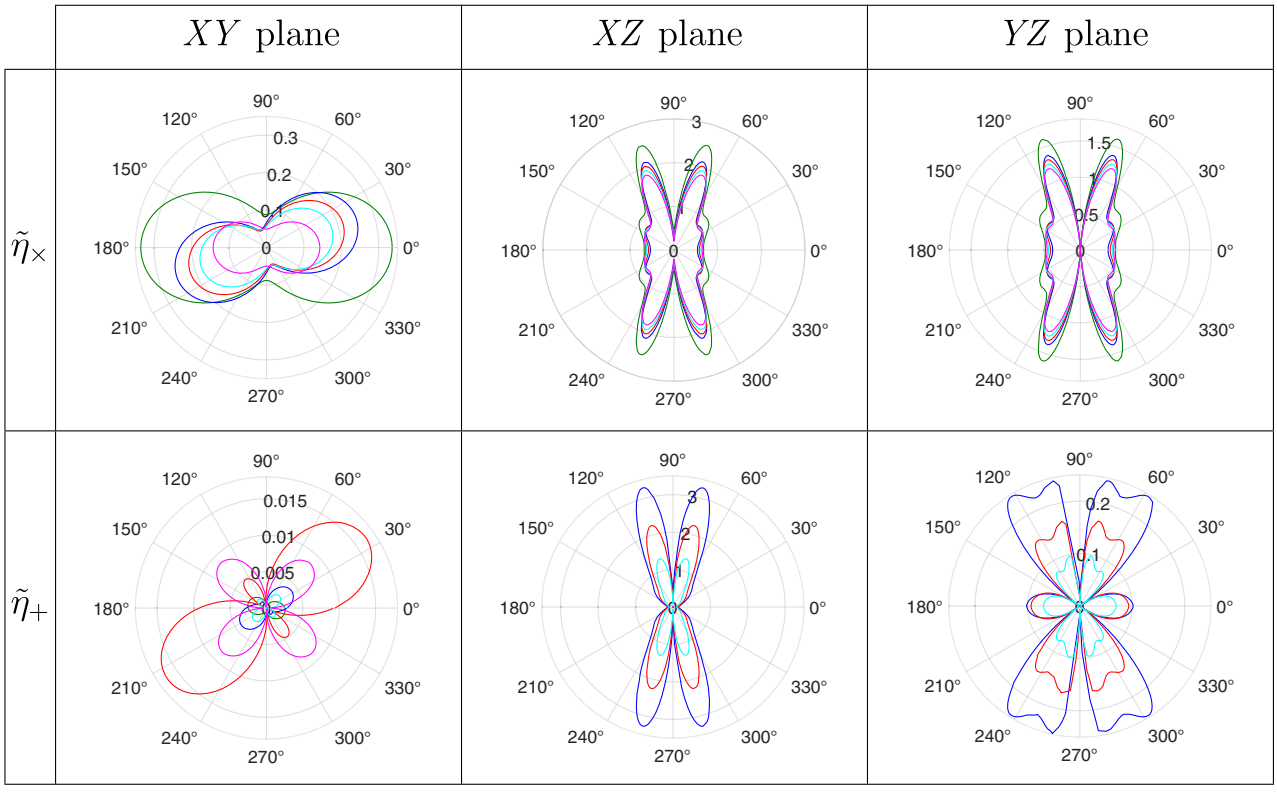


FIG. 7. Form factors for mode 1 in cavity 1 as a function of the incidence angle $\theta$. Rows make reference to the two different polarizations of the HFGW and columns make reference to the three different planes in which the incidence of the HFGW is studied. Each plates angle ($\alpha$) is illustrated with a different color: Green for $\alpha = 0°$, blue for $\alpha = 30°$, red for $\alpha = 45°$, cyan for $\alpha = 60°$, and magenta for $\alpha = 90°$. In the $\tilde{\eta}_+$ $XZ$ plane and $\tilde{\eta}_+$ $YZ$ plane cases $\alpha = 0°$ and $\alpha = 90°$ cannot be seen since the coupling is much lower in comparison to the rest of the angles. The same occurs for 0° in the $\tilde{\eta}_+$ $XY$ plane case.

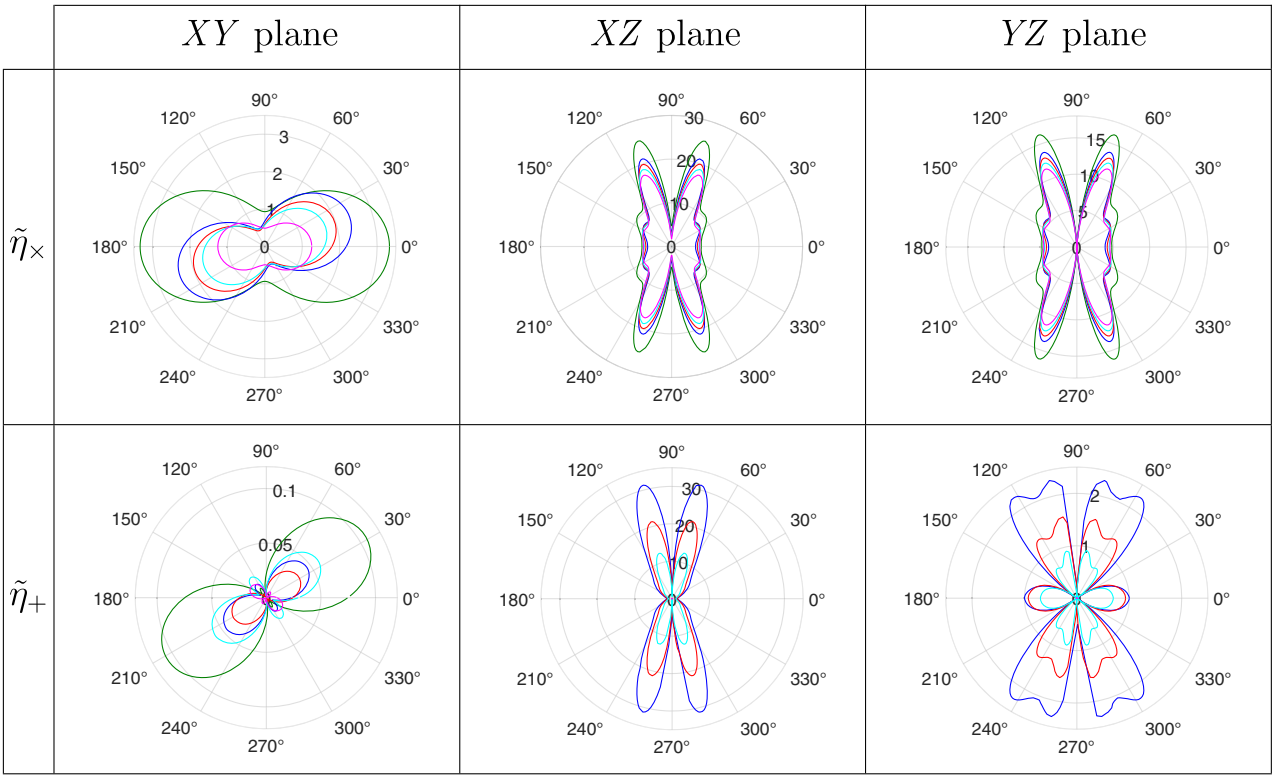


FIG. 8. Form factors for mode 1 in cavity 2 as a function of the incidence angle $\theta$. Rows make reference to the two different polarizations of the HFGW and columns make reference to the three different planes in which the incidence of the HFGW is studied. Each plates angle ($\alpha$) is illustrated with a different color: Green for $\alpha = 0°$, blue for $\alpha = 30°$, red for $\alpha = 45°$, cyan for $\alpha = 60°$, and magenta for $\alpha = 90°$. In the $\tilde{\eta}_+$ *XZ* plane and $\tilde{\eta}_+$ *YZ* plane cases 0° and $\alpha = 90°$ cannot be seen since the coupling is much lower in comparison to the rest of the angles.

another different value of $\alpha$ can be interpolated from the results shown here. The external magnetostatic field is assumed uniform, constant, and oriented towards the $y$ axis in the calculations [28]. The result of the form factor varies considerably with $\theta$, generating the kind of diagrams observed in Fig. 7 and 8. The existence of specific values of $\theta$ for which the system is blind to the incident HFGW is a crucial aspect of this analysis. In order to avoid these blind spots, daily modulation of the HFGW signal can be taken into account since the incidence angle of the gravitational wave will change and so will the form factor pattern, always provided that the source is stationary. In addition, studying more cavity modes that differ in their electric field structure can be useful to avoid blind spots [25]. An aspect associated with these angles of sensitivity drop is that their position in the polar plots does not vary considerably when changing the plates angle $\alpha$. Thus, one may employ two or more cavities oriented towards different directions in order to have full sky coverage.

A related aspect is the variation of the form factor $\tilde{\eta}$ with $\alpha$. There are cases where the system is more sensitive to an incident HFGW, as seen for instance in Figs. 7 and 8 when varying $\alpha$ from 0° (green) to 90° (magenta). These changes can be as big as an order of magnitude. As a consequence, when studying the coupling between a HFGW and a resonant microwave cavity, the influence of the tuning system is of special relevance. Moreover, this aspect not only affects the rf modal electric field, but also $\vec{J}_{+,\times}$ due to its dependence with frequency. This can be seen when comparing results of Fig. 8 with Fig. 7, where it is clear that not only an order of magnitude has been gained, but also a change in the pattern of the $\tilde{\eta}_+$ *XY* case can be seen.

The form factor for mode 2 has also been computed. Results are shown in Figs. 9 and 10. As it is seen in Fig. 2, initially ($\alpha = 0°$), this cavity mode has its rf electric field aligned with the $x$ axis, which implies a different effect on the form factor in the *XY* incidence plane during the frequency tuning. The cases $\alpha = 0°$ and $\alpha = 90°$ on $\tilde{\eta}_\times$ *XZ* and *YZ* planes are of special relevance due to the decrease of the form factor with respect to the rest of values of the angle $\alpha$, behavior that was also seen in the earlier tables of mode 1 but for the + polarization.

The same aspects discussed for mode 1 can be extrapolated for mode 2: the presence of blind spots for given values of $\theta$ in certain polarizations and incidence planes;

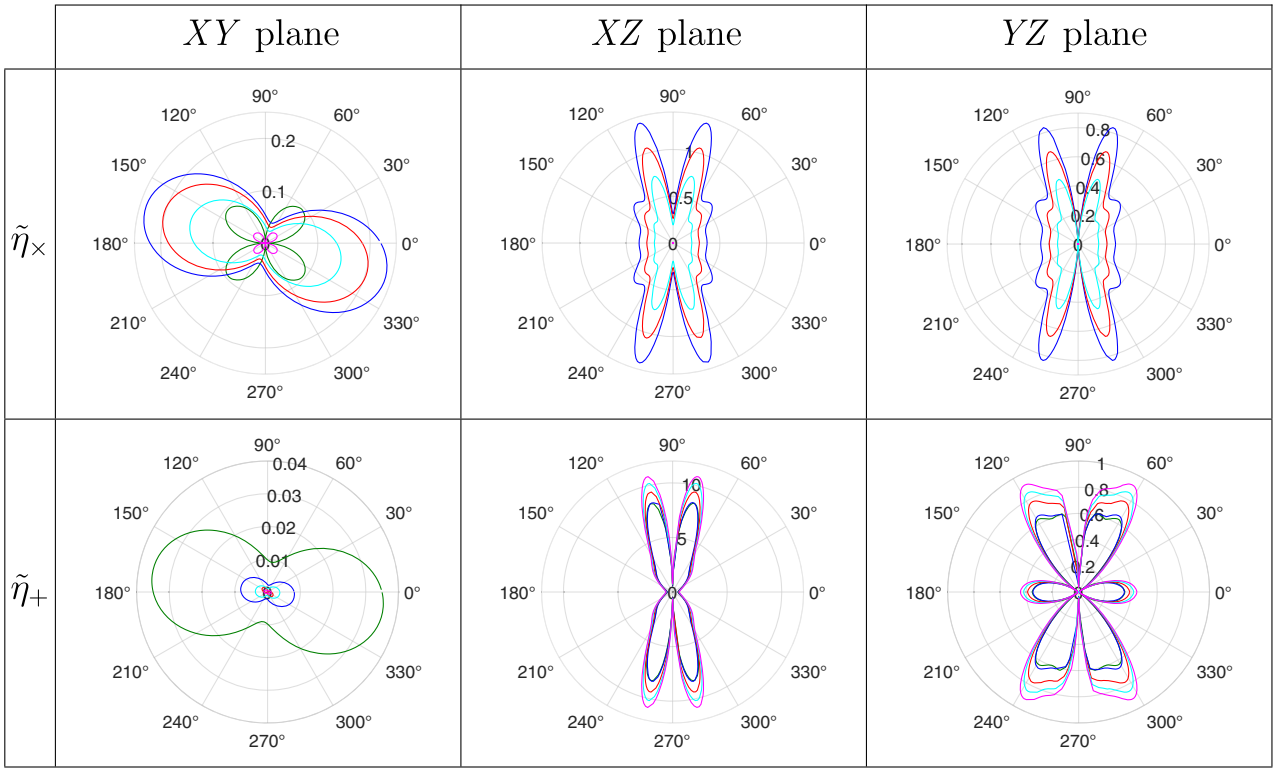


FIG. 9. Form factors for mode 2 in cavity 1 as a function of the incidence angle $\theta$. Rows make reference to the two different polarizations of the HFGW and columns make reference to the three different planes in which the incidence of the HFGW is studied. Each plates angle ($\alpha$) is illustrated with a different color: Green for $\alpha = 0°$, blue for $\alpha = 30°$, red for $\alpha = 45°$, cyan for $\alpha = 60°$, and magenta for $\alpha = 90°$. In the $\tilde{\eta}_\times$ $XZ$ plane and $\tilde{\eta}_\times$ $YZ$ plane cases $\alpha = 0°$ and $\alpha = 90°$ cannot be seen since the coupling is much lower in comparison to the rest of the angles. The same occurs with $\alpha = 30°$ and $\alpha = 90°$ form factor for $\tilde{\eta}_+$ $XY$ plane case.

the drastic change in the results when varying the plates angle, seen for instance in the $\tilde{\eta}_+$ $XY$ plane case (Fig. 9); and the change of the diagram pattern not only between the two different cavities studied but also with respect to mode 1.

The study of the form factor of mode 2 allows us to duplicate the scanning frequency range, due to the split evolution between modes 1 and 2 (see Fig. 3). Furthermore, it is key to assess the origin of the detected rf signal, as we now explain. Two situations are possible: both ports are excited; or only port 1 or port 2 is excited. The first case implies that the bandwidth of the detected rf signal is larger than the frequency gap between modes for a given angle of the plates. Since axions would not be able of exciting modes 1 and 2 at once due to its expected bandwidth [29], the signal could have been generated by a HFGW. If only port 1 is excited, then a study of the daily modulation of the signal must be performed in order to distinguish the cosmological source. Finally, if port 2 is excited alone, a consideration has to be taken into account. When varying the plates angle the electromagnetic field is being distorted, and as a consequence, an axion would be able to excite the second mode. Even though this coupling would be lower than the one of mode 1, it could be even more significant than the coupling of a HFGW due to its expected low amplitude. With that, it can be concluded that for this case a study of the time modulation of the rf signal would be also required.

Let us now be more explicit about the time variation of the signal, given its relevance to identify the kind of source behind the latter. For the axion case, the time modulation of the signal arises when considering the influence of the typical momentum of the axion field $\vec{k}_a$, introducing the spatial frequency term $\vec{k}_a \cdot \vec{r}$, where $\vec{r}$ is the spatial coordinates vector of the cavity. Since $\vec{k}_a$ is proportional to the velocity with which we see axions from our laboratory reference frame, the consideration of this term translates into a tiny daily modulation of the signal, suppressed by velocity $v \sim 10^{-3}c$ (being $c$ the speed of light in vacuum) of the axion galactic wind in our galaxy, as compared to the main rf signal [30,31]. Higher masses of the axion (higher momentum) and cavities of size comparable to the de Broglie wavelength maximize the influence of this term. Regarding HFGWs, the profile of the signal's time modulation strongly depends on which type of source produces the wave. For instance, if the signal is produced by the collision

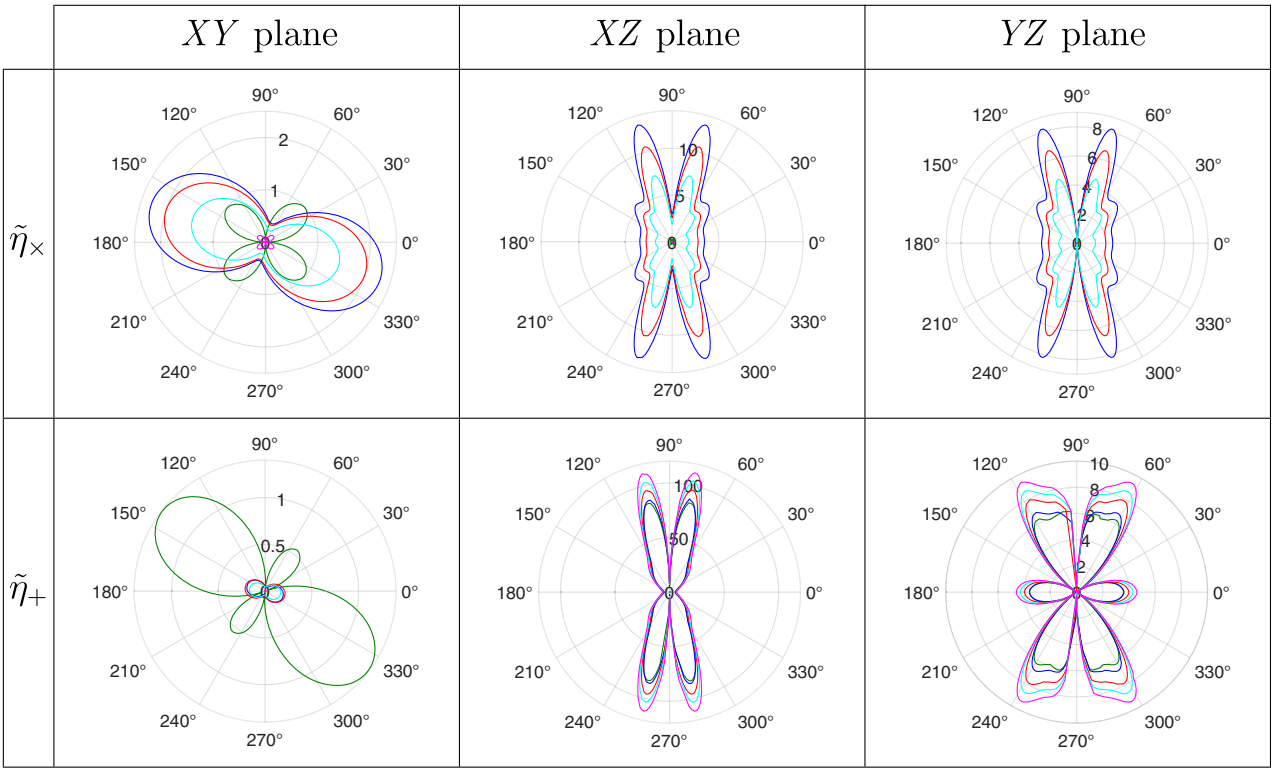


FIG. 10. Form factors for mode 2 in cavity 2 as a function of the incidence angle $\theta$. Rows make reference to the two different polarizations of the HFGW and columns make reference to the three different planes in which the incidence of the HFGW is studied. Each plates angle ($\alpha$) is illustrated with a different color: Green for $\alpha = 0°$, blue for $\alpha = 30°$, red for $\alpha = 45°$, cyan for $\alpha = 60°$, and magenta for $\alpha = 90°$. In the $\tilde{\eta}_\times$ $XZ$ plane and $\tilde{\eta}_\times$ $YZ$ plane cases $\alpha = 0°$ and $\alpha = 90°$ cannot be seen since the coupling is much lower in comparison to the rest of the angles.

between two primordial black holes, a chirping spectra is expected, and a signal duration which may be rather short [32,33]. Hence, the total time that the signal couples in band with a resonant mode has to be considered, in particular with respect to the tuning system employed in the experiment. Recall that changing the angle $\alpha$ of the plates inside the cavity modifies its resonant frequency, allowing us to sweep over a frequency range. If the HFGW bandwidth is high enough, a merging source may generate a signal in the cavity for more than one angle of plates $\alpha$. The fundamental question is how much time we integrate for a given value of $\alpha$. One solution would be to allow the system for fast readouts, where the frequency change when moving the plates from one angle to another is less than the frequency variation of the HFGW. However, the mechanical tuning system can take a few minutes to move from one of the angles studied to another, and this possibility seems unlikely. A more realistic strategy would be working with an array of cavities tuned to different frequencies for a simultaneous scan over a frequency range. This case is also favored, as the existence of chirping may be used as a way to confirm the origin of the signal, thus increasing detection prospects.

Finally, superradiant clouds associated to new bosons of mass $m_b$ can produce a stationary signal in our detector. These are long-lasting phenomena around spinning black holes of mass $M_{\rm BH} \sim (Gm_b)^{-1}$ ($G$ is Newton's constant) whose duration is over thousands of years and generate HFGWs in the band $\sim m_b$ [34]. Thus, the tuning system of our setup is ideal to search for this kind of sources. In this case, the rotation of the Earth would generate an $O(1)$ modification in the coefficients $\tilde{\eta}_{+,\times}$, from the relative rotation of $\vec{k}_{\rm GW}$ with respect to the cavity. Another source of persistent GWs is the stochastic backgrounds generated by several sources, possibly of primordial origin [2]. The treatment of the signals induced by GW backgrounds goes beyond the current analysis.

### A. Sensitivity estimation

At this point, a sensitivity estimation of the experiment can be made. The expected power generated by the HFGW inside the cavity can be expressed in Systeme International units as [5]

$$P_{\rm sig} = \frac{\varepsilon_0}{2} Q_{\rm eff} \omega_c^3 V^{5/3} (\tilde{\eta} h_0 B_0)^2, \tag{2}$$

where $\varepsilon_0$ is the vacuum electric permittivity; $Q_{\rm eff}$ is an effective quality factor; $\omega_c$ is the angular frequency of the HFGW; $V$ is the cavity volume; $h_0$ is the gravitational wave amplitude; and $B_0$ is the external static magnetic field. Since we do not have a specified source of interest, the value adopted by $Q_{\rm eff}$ will be the loaded cavity quality factor $Q_L$. Of course, when making this decision it is assumed that $Q_{\rm GW} \gg Q_L$ (where $Q_{\rm GW}$ is the quality factor of the GW), being in a situation in which the signal has been detected only in one port. From here, we can obtain the value of $h_0$ that can be reached taking into account Dicke's radiometer equation for the noise power [24], where $T_{\rm sys}$ is the sum of the noise temperature of the cavity, i.e., its physical temperature, and the noise temperature added by the readout chain, which is approximately that of the first amplifier; $k_B$ is the Boltzmann constant; $t_{\rm int}$ is the integration time; and $\Delta\nu$ is the frequency detection bandwidth:

$$\mathrm{SNR} = \frac{P_{\rm d}}{k_B T_{\rm sys}} \sqrt{\frac{t_{\rm int}}{\Delta\nu}}, \tag{3}$$

where $P_{\rm d} = \frac{\beta}{1+\beta} P_{\rm sig}$ is the detected power (recall that $\beta$ is the coupling coefficient [24]). By fixing SNR $> 3$,

$$h_0 > \frac{1}{\tilde{\eta} B_0} \left(\frac{\Delta\nu}{t_{\rm int}}\right)^{1/4} \left(\frac{1+\beta}{\beta} \frac{6 k_B T_{\rm sys}}{\varepsilon_0 Q_{\rm eff} \omega_c^3 V^{5/3}}\right)^{1/2}. \tag{4}$$

Employing the values for the case of cavity 1 with mode 1, $\alpha = 0°$ in the $XY$ plane for $\times$ polarization, and $\theta = 0°$ (which corresponds to the maximum form factor for this case), we obtain the sensitivity expectation,

$$h_0 > 9.38 \times 10^{-22} \left(\frac{\frac{1+\beta}{\beta}}{3/2}\right)^{1/2} \left(\frac{0.3356}{\tilde{\eta}}\right) \left(\frac{2\ \mathrm{T}}{B_0}\right) \left(\frac{\Delta\nu}{1.03\ \mathrm{kHz}} \frac{2\ \mathrm{min}}{t_{\rm int}}\right)^{1/4} \left(\frac{T_{\rm sys}}{4.6\mathrm{K}} \frac{96010}{Q_{\rm eff}}\right)^{1/2} \times \left(\frac{1.9 \times 10^9\ \mathrm{rad/s}}{\omega_c}\right)^{3/2} \left(\frac{1.1898 m^3}{V}\right)^{5/6}. \tag{5}$$

The value employed for the coupling factor, $\beta = 2$, is commonly used in axion haloscope experiments [35]. Since the form factors obtained in this work vary up to 2 orders of magnitude with respect to the one chosen for this calculation (as we have taken an average value, this variation can act to either enhance or suppress the rf signal by an order of magnitude), this must be considered just an illustrative example of the achievable sensitivity that the RADES-BabyIAXO setup can reach.

When referring to HFGW detection, contamination of the signal by noise coming from different sources always comes to mind. The methodology that will be followed for noise reduction is the same as other dark matter axion detection experiments: regarding thermal noise, it will be characterized, by means of the Y-method [24], intermittently throughout the data-taking campaign. In this way, the noise introduced by the system will be correctly assessed, such as the resonant noise of the cavity or the white noise introduced by the amplifier. Relating to vibrational noise, a study of the cavity resonant frequency stability must be performed. Referring to the magnetic field, a study of its effect on the measurements is made by carrying out the noise characterization mentioned above with the magnet switched on and off. Since the magnetic field can be the source of different kinds of systematic errors, this procedure can help to avoid false candidates in the analysis of the experiment results. In a realistic approach to the experiment, a typical readout chain as the ones employed in axion detection experiments would be applied, mainly composed by a circulator, an amplifier, a heterodyne receiver, and a vector network analyzer, as can be seen in [36–38].

The sensitivity of (6) may be improved in a number of ways: the integration time of 2 minutes may be extended, in particular considering the possibility of stationary sources of HFGW; lower temperatures inside the cryostat will be achievable with *DarkQuantum*, reaching temperatures up to tens of mK by the development of DL technologies and quantum limited amplification with SQUIDs; the considered unloaded quality factor of the cavity is the cryogenic one for pure copper, but this value can be improved by coating the cavity with superconducting materials such as rare-earth barium copper oxide or $Nb_3Sn$ [39]. The sensitivity expectations for both cavities and modes are shown in Table II. In each case, the employed value for the form factor corresponds to the maximum one of the $\tilde{\eta}_\times$ $XY$ plane cases.

The achievable sensitivities are still far away from the expected sources [40]. However, it should be remarked that these are the first steps in a dynamical field of research. When comparing with previous efforts [2], it can be seen that the BabyIAXO facility provides a

TABLE II. Sensitivity expectation of both cavities and modes for $h_0/10^{-21}$.

| | Mode 1 | Mode 2 |
|---|---|---|
| Cavity 1 | 0.94 | 4.00 |
| Cavity 2 | 5.45 | 23.01 |

TABLE III. Value of the figure of merit parameters employed for the sensitivity $h_0$ calculation. Values for the form factor $\tilde{\eta}$ correspond in each case to the incidence angle that maximizes the result in the $XY$ plane, and for $\alpha = 0°$ and cross polarization.

| | $\tilde{\eta}$ | $Q_l$ | $V$ (m$^3$) |
|---|---|---|---|
| Cavity 1, mode 1 ($\theta = 0°$) | 0.34 | 96010 | 1.20 |
| Cavity 1, mode 2 ($\theta = 317.4°$) | 0.10 | 71106 | 1.20 |
| Cavity 2, mode 1 ($\theta = 0°$) | 3.33 | 20970 | $1.10 \times 10^{-3}$ |
| Cavity 2, mode 2 ($\theta = 222.3°$) | 0.10 | 14955 | $1.10 \times 10^{-3}$ |

competitive sensitivity strain not only with respect to other cavity microwave experiments but also with respect to different detection techniques. Conservative values of the experimental parameters have been employed for our estimates, and there is much room for improvement of the experimental parameters in the coming years. For the sake of clarity, values of form factor, quality factor, and volume for each case, obtained from simulations, are shown in Table III.

Relative to signal processing, this is also an aspect where the same procedure can be followed as in other axion detection experiments. After time integration (which is favorable for stationary sources), possible candidates are selected. If possible, the integration time is increased to see if the candidates are just noise deviations or potential signals. If any of the candidates remain, a cross-correlation between the expected frequency distribution for the HFGW or the axion is performed. In addition, the magnet can be turned off to observe if any deviation is just a systematic introduced by this component of the setup. Furthermore, considering noise reduction in the analysis procedure, the application of the Savitzky-Golay filter has proven to be useful (as it can be seen in [38]). However, signal processing for HFGW detection in BabyIAXO is a topic that will be discussed in future work.

### B. Scanning rate

We can now perform a study of the scanning rate as is commonly made in axion experiments but particularizing it for the HFGW case. To deduce the detection rate expression, a similar approach to the one in [35,41] has been followed, obtaining

$$\frac{\mathrm{d}\nu}{\mathrm{d}t} = \left(\frac{\frac{\varepsilon_0}{2}\omega_c^3 V^{5/3}\tilde{\eta}^2 h_0^2 B_0^2}{\mathrm{SNR} k_B T_{\mathrm{cav}}}\right)^2 \left(\frac{\frac{\beta}{(1+\beta)}}{\frac{4\beta}{(1+\beta)^2}+\lambda}\right)^2 \frac{Q_{\mathrm{GW}}^3 Q_L}{(Q_{\mathrm{GW}}+Q_L)^2}, \tag{6}$$

where $\lambda = T_{\mathrm{amp}}/T_{\mathrm{cav}}$, with $T_{\mathrm{amp}}$ the temperature of the amplification stage and $T_{\mathrm{cav}}$ the physical temperature of the cavity. Using the same parameters employed in the sensitivity calculation section, this time in Eq. (6), we find the results shown in Table IV.

TABLE IV. Scanning rate of both cavities and modes in Hz/s.

| | Mode 1 | Mode 2 |
|---|---|---|
| Cavity 1 | 1.88 | 3.68 |
| Cavity 2 | 464.16 | 937.83 |

Even though these numbers have been derived for the mentioned experimental parameters, we must remark that they can vary considerably since, for instance, $\tilde{\eta}$ depends on the frequency of the incident signal.

The optimal $\beta$ in order to maximize this figure of merit can now be deduced, taking into account that $Q_L = \frac{Q_0}{1+\beta}$, where $Q_0$ is the unloaded quality factor of the cavity. The extreme of (6) will be achieved for the solution of

$$\lambda\beta^4 + (-4 + 2\lambda - \tilde{Q}\lambda)\beta^3 + (8 - 12\tilde{Q} + \lambda - 4\tilde{Q}\lambda)\beta^2 - 5\tilde{Q}\lambda\beta - 2\tilde{Q}\lambda = 0,$$

where $\tilde{Q} = \frac{Q_0}{Q_{\mathrm{GW}}} + 1$. The result strongly depends on the values that $\lambda$ and $\tilde{Q}$ adopt as it can be seen in Fig. 11. In dark matter axion detection with haloscopes, one sets $\beta_{\mathrm{opt}} = 2$, which is obtained when considering $\lambda \gg 1$ and $\tilde{Q} \approx 1$. However, for the case of BabyIAXO, due to quantum limited amplification with SQUIDs and other technologies, in the coming years it would be able to decrease $\lambda$ and increase $\tilde{Q}$. In this way, representative values for this parameters taking into account these expectations in quantum technology would be $\lambda = 5$ and $\tilde{Q} = 2$, thus obtaining an optimum coupling $\beta_{\mathrm{opt}} = 4$. This $\beta$ is reached by fixing $\varphi_1$ and $\varphi_2$ to the appropriate value. However, coaxial loops are a strongly sensitive device that

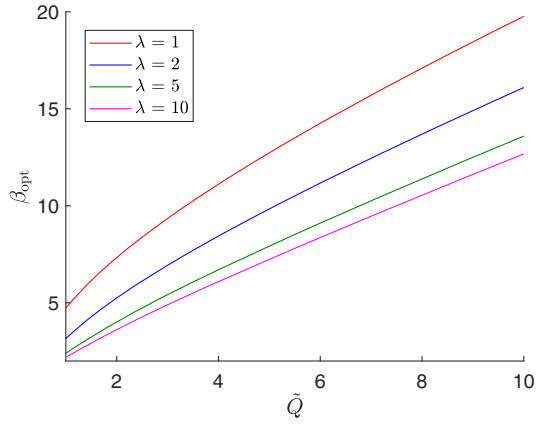


FIG. 11. Behavior of the optimum coupling factor $\beta_{\mathrm{opt}}$ when varying $\lambda$ and $\tilde{Q}$.

require a fine-tuning depending on the real pattern of the electromagnetic field.

## V. CONCLUSIONS

This article examines the possibilities of using RADES-BabyIAXO haloscope and a scaled version for higher frequencies as HFGW detectors. For that, a calculation of the form factor between HFGW and two RADES-BabyIAXO cavities has been performed, analogously to the dark matter axion case outlined in [25]. The complexity of the electric current density generated by the HFGW implies the coupling to a different set of modes supported by the cavity. Two orthonormal quasi-$TE_{111}$ modes have been studied, obtaining different results for the two HFGW polarizations, as well as for different planes and angles of incidence. A novel approach to the HFGW detection has been proposed in this work, since it is the first time that the simultaneous detection of axion and HFGWs has been studied. In addition, a realistic setup has been considered by incorporating the presence of tuning plates and coupling ports inside the cavity.

We have shown the relevance of this tuning system by observing the drastic change in the form factor when varying the plates angle. In addition, a sensitivity estimation of both cavities has been calculated, obtaining for both modes values of $h_0 \sim 10^{-21}$ for cavity 1 and of $h_0 \sim 10^{-20}$ for cavity 2 (cf. Table II). Having followed the same methodology as in previously published work, these values are deemed reliable and could be considerably improved via optimization of the experimental parameters, with the final goal of achieving sensitivities closer to that of possible rf signals. Moreover, a qualitative study on how to distinguish a signal generated by a HFGW or an axion has been developed, concluding that RADES-BabyIAXO cavities are capable of distinguishing both cases, in the case of stationary signals. The study of the form factor has been made for two orthonormal modes of both cavities, concluding that these two modes can be used for HFGW detection and, therefore, achieve a duplication of the scanning frequency range. Our study can be easily expanded to other higher-order resonant modes, provided that the cavity contains the appropriate probes (loops or monopoles) for these modes. Moreover, the scanning rate has been derived in Eq. (6), following a similar approach to that of the axion case. This allows to compute the optimal coupling factor $\beta$ maximizing the detection rate. The ideal HFGW scenario for the RADES-BabyIAXO setup are stationary sources, as superradiant black holes or stochastic GWs backgrounds (the latter is not considered in this study). Nevertheless, transient waves can also be detected even though this depends on the bandwidth of the HFGW.

In conclusion, BabyIAXO has potential to be employed as a HFGW detector, while still being used as a dark matter axion detector. Since BabyIAXO is an experiment under development, we have shown that it can be adapted with minor modifications to detect HFGWs. Regarding future directions, the employment of these cavities for an up-down conversion-type detector can be considered, similarly to [6,37]. In these setups, the resonant cavity is fed by a pump mode and the presence of an axion or a HFGW can generate a signal in a readout mode. As the frequency gap between mode 1 and mode 2 can be small [42], the up-down conversion may be useful to explore HFGWs of frequencies below those considered in this work. By changing the plates angle, scanning to higher frequencies can be done since the gap between modes increases. Thus, RADES-BabyIAXO setup has a high capacity to be also considered as an up-down conversion detector.

## ACKNOWLEDGMENTS

This work was performed within the RADES group. We thank our colleagues for their support, especially Camilo García Cely for providing us with the currents expressions and his useful comments. Thanks also to Pablo Martín Luna for his valuable comments and discussions. The research leading to these results has received funding from the Spanish Ministry of Science and Innovation with Projects No. PID2020–115845 GB-I00/AEI/10.13039/501100011033, No. PID2022-137268NBC53 and No. PID2022-137268NA-C55, funded by MICIU/AEI/10.13039/501100011033/ and by "ERDF/EU." I. F. A. E. is partially funded by the CERCA program of the Generalitat de Catalunya. J. Reina-Valero has the support of "Plan de Recuperación, Transformación y Resiliencia (PRTR) 2022 (ASFAE/2022/013)," funded by Conselleria d'Innovació, Universitats, Ciència i Societat Digital from Generalitat Valenciana, and NextGenerationEU from European Union. D. B. acknowledges the support from the Departament de Recerca i Universitats from Generalitat de Catalunya to the Grup de Recerca 00649 (Codi: 2021 SGR 00649). I. G. I. acknowledges support from the European Union's Horizon 2020 research and innovation program under the European Research Council (ERC) Grant Agreement No. ERC-2017-AdG788781 (IAXO+), as well as from the "European Union NextGenerationEU/PRTR" (Planes complementarios, Programa de Astrofísica y Física de Altas Energías).

[1] B. P. Abbott *et al.* (LIGO Scientific and Virgo Collaborations), Observation of gravitational waves from a binary black hole merger, Phys. Rev. Lett. **116**, 061102 (2016).

[2] N. Aggarwal *et al.*, Challenges and opportunities of gravitational-wave searches at MHz to GHz frequencies, Living Rev. Relativity **24**, 4 (2021).

[3] M. Gertsenshtein, Wave resonance of light and gravitional waves, Sov. Phys. JETP **14**, 84 (1962).

[4] M. E. Gertsenshtein and V. I. Pustovŏit, On the detection of low frequency gravitational waves, Sov. Phys. JETP **16**, 433 (1962).

[5] A. Berlin, D. Blas, R. Tito D'Agnolo, S. A. R. Ellis, R. Harnik, Y. Kahn, and J. Schütte-Engel, Detecting high-frequency gravitational waves with microwave cavities, Phys. Rev. D **105**, 116011 (2022).

[6] A. Berlin, D. Blas, R. Tito D'Agnolo, S. A. R. Ellis, R. Harnik, Y. Kahn, J. Schütte-Engel, and M. Wentzel, Electromagnetic cavities as mechanical bars for gravitational waves, Phys. Rev. D **108**, 084058 (2023).

[7] W. Ratzinger, S. Schenk, and P. Schwaller, A coordinate-independent formalism for detecting high-frequency gravitational waves, J. High Energy Phys. 08 (2024) 195.

[8] R. D. Peccei and H. R. Quinn, CP conservation in the presence of pseudoparticles, Phys. Rev. Lett. **38**, 1440 (1977).

[9] J. E. Kim and G. Carosi, Axions and the strong *CP* problem, Rev. Mod. Phys. **82**, 557 (2010); Rev. Mod. Phys. **91**, 049902(E) (2019).

[10] H. Primakoff, Photoproduction of neutral mesons in nuclear electric fields and the mean life of the neutral meson, Phys. Rev. **81**, 899 (1951).

[11] P. Sikivie, Detection rates for "invisible"-axion searches, Phys. Rev. D **32**, 2988 (1985).

[12] N. Du *et al.* (ADMX Collaboration), A search for invisible axion dark matter with the axion dark matter experiment, Phys. Rev. Lett. **120**, 151301 (2018).

[13] C. M. Adair *et al.*, Search for dark matter axions with CAST-CAPP, Nat. Commun. **13**, 6180 (2022).

[14] K. M. Backes *et al.* (HAYSTAC Collaboration), A quantum-enhanced search for dark matter axions, Nature (London) **590**, 238 (2021).

[15] R. Barbieri, C. Braggio, G. Carugno, C. Gallo, A. Lombardi, A. Ortolan, R. Pengo, G. Ruoso, and C. Speake, Searching for galactic axions through magnetized media: The QUAX proposal, Phys. Dark Universe **15**, 135 (2017).

[16] A. Álvarez Melcón, S. A. Cuendis, C. Cogollos, A. Díaz-Morcillo, B. Döbrich, J. D. Gallego, B. Gimeno, I. G. Irastorza, A. J. Lozano-Guerrero, C. Malbrunot, P. Navarro, C. P. Garay, J. Redondo, T. Vafeiadis, and W. Wuensch, Axion searches with microwave filters: The RADES project, J. Cosmol. Astropart. Phys. 05 (2018) 040.

[17] B. Aja *et al.*, The Canfranc Axion Detection Experiment (CADEx): Search for axions at 90 GHz with kinetic inductance detectors, J. Cosmol. Astropart. Phys. 11 (2022) 044.

[18] B. T. McAllister, G. Flower, E. N. Ivanov, M. Goryachev, J. Bourhill, and M. E. Tobar, The ORGAN experiment: An axion haloscope above 15 GHz, Phys. Dark Universe **18**, 67 (2017).

[19] E. Armengaud *et al.*, Conceptual design of the International Axion Observatory (IAXO), J. Instrum. **9**, T05002 (2014).

[20] E. Armengaud *et al.* (IAXO Collaboration), Physics potential of the International Axion Observatory (IAXO), J. Cosmol. Astropart. Phys. 06 (2019) 047.

[21] A. Abeln *et al.*, Conceptual design of BabyIAXO, the intermediate stage towards the International Axion Observatory, J. High Energy Phys. 05 (2021) 137.

[22] S. Ahyoune *et al.*, A proposal for a low-frequency axion search in the 1-2 μeV range and below with the BabyIAXO magnet, Ann. Phys. (Berlin) **535**, 2300326 (2023).

[23] M. Siodlaczek, Thermodynamic design of a cryostat for a radiofrequency cavity detector in BabyIAXO in search of dark matter, Master's thesis, CERN, 2022.

[24] D. M. Pozar, *Microwave Engineering*, 3rd ed. (Wiley, Hoboken, NJ, 2005).

[25] P. Navarro, B. Gimeno, J. Monzó-Cabrera, A. Diaz-Morcillo, and D. Blas, Study of a cubic cavity resonator for gravitational waves detection in the microwave frequency range, Phys. Rev. D **109**, 104048 (2024).

[26] V. Domcke, C. Garcia-Cely, and N. L. Rodd, Novel search for high-frequency gravitational waves with low-mass axion haloscopes, Phys. Rev. Lett. **129**, 041101 (2022).

[27] CST AG, CST studio suite, versión 2024 (2024), https://www.3ds.com/products-services/simulia/products/cst-studio-suite/.

[28] Nevertheless, as can be seen in [22], since it has some distortions in the external part of the bore, the magnetic field of the BabyIAXO experiment is not completely uniform. This aspect is more relevant in Cavity 1 since its dimensions are higher.

[29] Excluding the possibility of two axions with a mass split corresponding to the one between both modes.

[30] S. Knirck, A. J. Millar, C. A. O'Hare, J. Redondo, and F. D. Steffen, Directional axion detection, J. Cosmol. Astropart. Phys. 11 (2018) 051.

[31] I. G. Irastorza and J. A. García, Direct detection of dark matter axions with directional sensitivity, J. Cosmol. Astropart. Phys. 10 (2012) 022.

[32] M. Maggiore, *Gravitational Waves. Vol. 1: Theory and Experiments*, Oxford Master Series in Physics (Oxford University Press, New York, 2007).

[33] G. Franciolini, A. Maharana, and F. Muia, Hunt for light primordial black hole dark matter with ultrahigh-frequency gravitational waves, Phys. Rev. D **106**, 103520 (2022).

[34] R. Brito, V. Cardoso, and P. Pani, Superradiance: New frontiers in black hole physics, Lect. Notes Phys. **906**, 1 (2015).

[35] D. Kim, J. Jeong, S. Youn, Y. Kim, and Y. K. Semertzidis, Revisiting the detection rate for axion haloscopes, J. Cosmol. Astropart. Phys. 03 (2020) 066.

[36] R. Khatiwada, D. Bowring, A. Chou, A. Sonnenschein, W. Wester, D. Mitchell, T. Braine, C. Bartram, R. Cervantes, N. Crisosto *et al.*, Axion dark matter experiment: Detailed design and operations, Rev. Sci. Instrum. **92** (2021).

[37] C. A. Thomson, M. Goryachev, B. T. McAllister, E. N. Ivanov, P. Altin, and M. E. Tobar, Searching for low-mass axions using resonant upconversion, Phys. Rev. D **107**, 112003 (2023).

[38] S. Ahyoune *et al.*, RADES axion search results with a high-temperature superconducting cavity in an 11.7 t magnet, arXiv:2403.07790.

[39] J. Golm *et al.*, Thin film (high temperature) superconducting radiofrequency cavities for the search of axion dark matter, IEEE Trans. Appl. Supercond. **32**, 1 (2022).

[40] C. Gatti, L. Visinelli, and M. Zantedeschi, Cavity detection of gravitational waves: Where do we stand?, Phys. Rev. D **110**, 023018 (2024).

[41] A. Díaz-Morcillo, J. M. García Barceló, A. J. Lozano Guerrero, P. Navarro, B. Gimeno, S. Arguedas Cuendis, A. Álvarez Melcón, C. Cogollos, S. Calatroni, B. Döbrich, J. D. Gallego-Puyol, J. Golm, I. G. Irastorza, C. Malbrunot, J. Miralda-Escudé, C. Peña Garay, J. Redondo, and W. Wuensch, Design of new resonant haloscopes in the search for the dark matter axion: A review of the first steps in the RADES Collaboration, Universe **8**, 5 (2022).

[42] This is seen in Fig. 3. However, via a optimization of the cavity dimensions this frequency gap can be set to any desired value.